ROLE OF SHORT-PULSE LASER FOR DETECTION AND DIFFERENTIATION OF CANCER STAGES AND BENIGN LESION WITHIN HUMAN SKIN

Bhowmik A.[1], Repaka R.[2,*], and Mishra S.C.[3]
*Author for correspondence
[1]Mechanical and Aerospace Engineering Department,
University of California, Los Angeles, California-90095, USA
[2]School of Mechanical, Materials and Energy Engineering,
Indian Institute of Technology Ropar, Rupnagar-140001, Punjab, India
[3]Department of Mechanical Engineering,
Indian Institute of Technology Guwahati, Guwahati-781039, Assam, India
E-mail: ramjee.repaka@iitrpr.ac.in

ABSTRACT

The present study pertains to theoretical evaluation of various skin lesions using reflectance mode short-pulse (SP) laser technique, which has been assumed to be operating within the therapeutic optical window of 600-1300 nm. The skin and lesions have been modeled based on anatomic details and optical properties available in the literature. Whereas, the different lesion stages have been modeled according to the American Joint Committee for Cancer Staging guidelines. The numerical simulation of transient radiative transfer equation has been carried out with the aid of finite volume method (used for resolving angular and spatial distributions) and backward differencing formula (used for time discretization). The anisotropic scattering of diffuse light due to the attenuation of incident laser light has been demonstrated using Henyey-Greenstein scattering phase function. The numerical analysis revealed that the associated changes in reflected radiative signatures due to the change in tissue properties (i.e. for different form of skin lesions) and conditions (i.e., growth features) can be a means to detect and differentiate the skin cancer.

INTRODUCTION

Cancer is a disease that leads to genetically damaged genes, i.e., oncogenes, causing them to proliferate and mutate. These cells are capable to double its volume faster in an uncontrollable manner assisted by an increase in metabolic activities. Skin cancers on the other hand are frequently found cancers among the patients around the world. According to the world health organization, the incident rate of skin cancer increases each year in the western countries, and the reported data suggests nearly 3 million cases of non-melanoma and 132000 cases of melanoma occur every year globally. Among all forms of skin cancers, the melanoma of the skin causes majority of the deaths and are capable to metastasize rapidly. Thus, it is important that melanoma of skin has to be detected as well as differentiated from other lesions as early as possible.

At present in most clinical settings [1] the detection of skin cancer relies on (a) naked-eye examination of morphological features using the classical ABCDE rule, and (b) using subsurface feature extraction methods, viz., total body photography, digital and polarized light dermoscopes. Nevertheless, till the date, the surgical excision and pathological studies have been considered as the golden standard to ascertain its possibility and condition [2]. Currently many new in-vivo microscopic and non-invasive imaging modalities are explored all over the world to detect the traces of skin melanoma. These modalities are (a) in-vivo microscopic imaging, viz., high end magnification devices such as binocular microscopes and video microscopy [3], confocal scanning laser microscopy working in both reflectance and fluorescence modes [4, 5], etc., and (b) non-invasive imaging modalities, viz., multispectral imaging (MelaFind) [6], optical coherence tomography, computerized tomography, magnetic resonance imaging, positron emission tomography, single-photon emission computed tomography, diffuse optical tomography [7], ultrasound [8], photo-acoustic imaging [9], Raman spectroscopy method [10], fluorescence spectroscopy [11] and thermal imaging [12], and many more. A detailed description of various clinical methods used for melanoma diagnosis has been elaborated in ref. [1].

In spite of all the above techniques for skin cancer detection, recently the optical [7, 13-15], thermal [12] and acoustic [9] techniques have drawn the interest of many researchers for the detection of skin cancer. Since, these techniques are fast, simple, safe, relatively inexpensive, easy to handle, and can suggest important patho-physiological phenomena of cancer which remain unwrapped in other methods. The newly developed optical modality has been believed to be useful tool for the detection and differentiation of skin cancer [15]. Therefore, the present work uses the reflectance mode short-pulse (SP) laser for the detection and differentiation of cancer stages from healthy skin and benign lesion. The methodology uses a SP laser source with proper time gating detection technique to capture the small temporal reflected radiative signatures emanating from the tissue. The objective of the present numerical study is to verify the performance of the reflectance mode SP laser for the detection and differentiation of skin cancer stages, as well as identify the distinguishing features of benign lesion. This study uses finite

volume method (FVM) for numerical analysis compared to modified discrete ordinate method (mDOM) [15]. This technique has inherent advantages of being fast, safe (non-ionizing) and can provide information of early trends of malignancies which remains unwrapped in other techniques. In order to materialize the argument described above, the present work performs an extensive numerical investigation on an approximated human skin model embedded with abnormalities of different growth phases.

NOMENCLATURE

c	[m/s]	Speed of light in medium
d	[m]	Depth
I	[W/m^2]	Intensity
I_b	[W/m^2]	Black body intensity $\left(=\sigma T_t^4/\pi\right)$
Ic	[W/m^2]	Collimated intensity
L	[-]	Order of approximation of Legendre polynomial
S	[-]	Source term
T_p	[s]	Time period of pulse train
T_t	[K]	Tissue temperature
V	[m^3]	Volume of cell
g	[-]	Anisotropic factor
n	[-]	Refractive index
q	[W/m^2]	Heat flux
$\vec{r}$	[-]	Position vector
s	[m]	Geometric distance in the direction of intensity $\hat{s}$
t	[s]	Time
t_p	[s]	Pulse width
t_c	[s]	Cut-off period
z	[m]	Physical thickness

Special characters

κ_a	[1/m]	Absorption coefficient
σ	[W/m^2 K^4]	Stefan-Boltzmann constant (= 5.64x10^{-8} W/m^2 K^4)
σ_s	[1/m]	Scattering coefficient
β	[1/m]	Extinction coefficient
θ	[-]	Polar angle
φ	[-]	Azimuthal angle
ε	[-]	Emissivity
δ	[-]	Dirac-delta function
Ω	[-]	Solid angle, (θ,φ)
$\Delta\Omega$	[-]	Elemental solid angle

Subscripts

c	Collimated
d	Diffuse
i	Incident
l	Lesion
$norm$	Normal
N, S	North and South
P	Cell centre
ref	reflectance
t	Total
vac	Vacuum
w	Wall

Superscripts

m	Index for discrete directions
$*$	Non-dimensional parameters

PROBLEM DEFINITION

The study has been carried out by considering human skin models with benign skin lesion, viz., dysplastic nevi (DPN) and different stages of cutaneous melanoma (CM). Figure 1 depicts the schematic of human skin model, and Fig. 2 depicts the staging of T1 melanoma in human skin as was suggested by American Joint Committee for Cancer staging (AJCCS) [16]. Human skin consists of three layers as shown in Fig. 1. The outer layer exposed to environment is the epidermis. The layer below the living epidermis is known as dermis. The layer below the dermis is the fatty layer. The harmful CM initially originates from the melanocytes located within the basal layer at the junction of living epidermis and papillary dermis (Fig. 1).

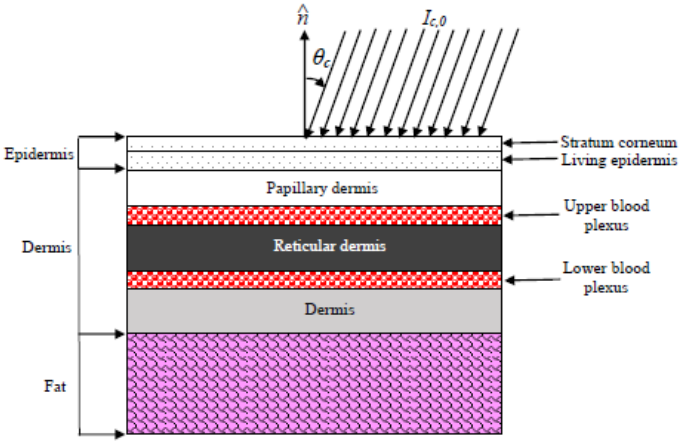

Figure 1 Schematic of human skin ($\hat{n}$ is the outward normal, $I_{c,0}$ is the maximum intensity of collimated ray and θ_c is the angle of incidence).

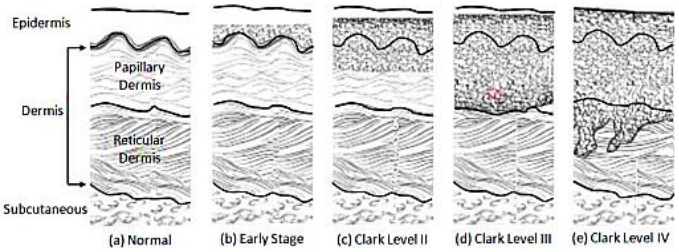

Figure 2 Staging of T1 melanoma within the skin (Image courtesy [16]).

The thickness and optical properties of normal [17-19] and abnormal tissues [20] were shown in Table 1. The DPN and CM at its early stage have been modelled within the constituting layer, i.e., basal layer (10 μm thick at the junction of living epidermis and papillary dermis). Later, the CM has been staged according to the skin cancer staging specifications given by AJCCS guidelines [16]. Based on penetration of T1 melanoma in the skin, the three Clark levels (CL) of melanoma, viz., CL II, III and IV have been considered in the present investigation. The penetration of CM to portion of papillary dermis (110 μm), complete papillary dermis (150 μm) and portion of reticular dermis (760 μm) have been levelled as different Clark levels, viz., CL II, CL III and CL IV, respectively [16]. The dysplastic nevi (DPN) and early stage of

melanoma (ES I) have been modelled at the junction of epidermis and dermis (within the basal layer having 10 μm thickness). The DPN is a benign case, which grow relatively slow compared to the melanoma, and therefore the dimension is kept constant compared to the growth of melanoma.

Table 1 Optical properties of skin tissues and skin cancer at 785 nm [17-20].

Tissues	d (mm)	β (mm^{-1})	σ_S (mm^{-1})	g
Stratum corneum	0.01	18.95089	18.95	0.8
Living epidermis	0.08	19.14	18.95	0.8
Papillary dermis	0.1	11.78	11.65	0.8
Upper blood plexus	0.08	15.64375	15.485	0.818
Reticular dermis	1.50	11.78	11.65	0.8
Deep blood plexus	0.07	46.85375	46.165	0.962
Dermis	0.16	11.78	11.65	0.8
Fat	3.0	11.448	11.44	0.9
Cutaneous melanoma (CM)	--	9.1925	9.185	0.8-0.9
Dysplastic nevi (DPN)	--	7.122	6.980	0.8

MATHEMATICAL MODEL AND NUMERICAL METHOD

The generalized governing equation for the transport of light within an absorbing, emitting and scattering tissue in any direction ŝ about the elemental solid angle ΔΩ is given as [7, 13-15, 21, 22]

$$\frac{1}{c}\frac{\partial I(r,\hat{s},t)}{\partial t}+\frac{dI(r,\hat{s},t)}{ds}=-\beta(r)I(r,\hat{s},t)+\kappa_a(r)I_b(r,\hat{s},t)+\frac{\sigma_s(r)}{4\pi}\int_{\Omega=4\pi} I(r,\hat{s}_i,t)\Phi(\hat{s},\hat{s}_i)\,d\Omega_i \quad (1)$$

where I is the intensity which is a function of direction Ω(θ, ϕ) and wavelength λ, ΔΩ is the solid angle (= sinθ $d\theta$ $d\phi$), θ is the polar angle, ϕ is the azimuthal angle, r is the position vector, t is the time, $\hat{s}$ is the direction vector, s is the geometrical distance in the direction $\hat{s}$, c is the speed of light in the medium (= c_{vac}/n), c_{vac} is the speed of light in vacuum, n is the refractive index (= 1.4), β is the extinction coefficient (=κ_a + σ_s), κ_a is the linear absorption coefficient, σ_s is the linear scattering coefficient, I_b is the black body intensity, $\Phi(\hat{s}, \hat{s}_i)$ is the scattering phase function and subscript i denoted incident directions. The tissue is approximated as 1-d planar participating medium (Fig. 1) and a longitudinal section of tissue has been considered.

The propagation of collimated component of laser light is given as [22]:

$$\left(\frac{1}{c}\right)\frac{\partial I_c(r,\hat{s},t)}{\partial t}+\frac{\partial I_c(r,\hat{s},t)}{\partial s}=-\beta(r)I_c(r,\hat{s},t) \quad (2)$$

The diffuse intensity I_d within the medium originates due to the attenuation of collimated intensity of laser, I_c Thus, the intensity I in Eq. (1) is composed of two components, i.e., $I = I_c + I_d$. Substituting the expressions for intensity I as well as equation for collimated intensity I_c (i.e., Eq. (2)) in Eq. (1), give rise to a modified radiative transfer equation (RTE) [15]

$$\left(\frac{1}{c}\right)\frac{\partial I_d(r,\hat{s},t)}{\partial t}+\frac{dI_d(r,\hat{s},t)}{ds}=-\beta(r)I_d(r,\hat{s},t)+S_t(r,\hat{s},t) \quad (3)$$

where S_c and S_d are the source terms due to the collimated and diffuse radiations, respectively, and S_t (= S_c + S_d) is the total source term. The source term due to collimated and diffuse remnant can be written as [15, 22]

$$S_c(r,\hat{s},t)=\frac{\sigma_s(r)}{4\pi}\int_{4\pi} I_c(r,\hat{s}_i,t)\Phi(\hat{s},\hat{s}_i)\,d\Omega_i$$
$$S_d(r,\hat{s},t)=\kappa_a(r)I_b(r,t)+\frac{\sigma_s(r)}{4\pi}\int_{4\pi} I_d(r,\hat{s}_i,t)\Phi(\hat{s},\hat{s}_i)\,d\Omega_i \quad (4)$$

With θ_c, the incident angle of the laser source measured from the outward normal to the north boundary (Fig. 1), the collimated intensity (I_c) in Eq. (4) can be written as [15, 23]

$$I_c(r,\hat{s},t)=I_{c,0}(\hat{s},t)e^{-\beta(r)s_c}\,e^{\left[-4\ln 2\left(\frac{t-\frac{s_c}{c}-t_c-(N-1)T_p}{t_p}\right)^2\right]}\times\delta(\theta-\theta_c) \quad (5)$$

where $I_{c,0}$ is the maximum laser intensity at the skin surface, s_c = z/cosθ_c is the geometric distance in the direction Ωc(θ_c), N is the number of pulses, T_p (=2 t_c) is the time period, t_c = 3t_p is the cut-off time, t_p is the pulse width and δ is the Dirac-delta function.

The scattering phenomenon in the biological medium is mostly in the forward direction, due to which the scattering phase function, $\Phi(\hat{s}, \hat{s}_i)$ in Eq. (4) is approximated using Henyey-Greenstein (H-G) phase function [15, 21]. The H-G scattering phase function can be written in terms of Legendre polynomial, P_L, for azimuth symmetric case and is given as:

$$\Phi(\hat{s},\hat{s}_i)=1+\sum_{L=1}^{L\,max}(2L+1)g^L P_L(\cos\theta)\,P_L(\cos\theta_i) \quad (6)$$

where g is the asymmetry factor/average cosine of the phase function, L is the order of approximation, ŝ and ŝ$_i$ are the direction vectors. The study considers Legendre polynomial of 18th order, i.e., L_{max} = 18. It is fair enough to have this approximation, since, the change in the solutions is minute for L > 18. The boundary intensity is given as [22]:

$$I_d(r_w,\hat{s},t)=\frac{\varepsilon_w\sigma T_w^4}{\pi}+\left(\frac{1-\varepsilon_w}{\pi}\right)\int_{\hat{n}_w\bullet\hat{s}<0}\left[I_d(r_w,\hat{s},t)+I_c(r_w,\hat{s},t)\right]\cos\theta\,d\Omega \quad (7)$$

where T_w, ε_w and σ represent the boundary temperature, the wall emissivity and the Stefan-Boltzmann constant, respectively, subscript w represents the wall or the skin

boundary. The first term on the right hand side of Eq. (7) represents the emitted intensity from the boundary and second term represents the reflected component of the boundary intensity.

The diffuse intensity I_d in the medium can be obtained by solving Eq. (3) along with the knowledge of source term S_t from Eq. (4). Variation of the collimated intensity (I_c) within the tissue can be obtained by solving Eq. (5). It has to be noted that, the evaluation of the source term S_t (= S_c + S_d) requires the knowledge of intensity distributions, I_c and I_d. After the intensities are estimated at all nodes and discrete angles using Eqs. (3) and (7), the radiative heat flux values could be determined using [22]

$$q_j(r,t) = \int_{4\pi} I_j(r,\Omega_i,t)\cos\theta_i\, d\Omega_i \tag{8}$$

where subscript j is a variable representing either collimated, c or diffuse, d. The reflected radiative signature is mainly due to the scattered intensity measured at the irradiated skin surface and can be written in non-dimensional form as [22]:

$$q^*_{ref}(r_N,t) = \frac{q_d(r_N,t)}{q_{c,0}(r_N,t)} \tag{9}$$

where q_d is the heat flux due to diffuse remnant and $q_{c,0}$ is the maximum heat flux at the irradiated boundary r_N (say, north boundary is irradiated).

In the present study, fully implicit numerical procedure has been adopted. The FVM has been used in this work to evaluate the transient intensities in all the discrete directions, say m, by following a specific set of time marching and ray tracing methods [22]. At first, the modified RTE (Eq. (3)) has been written for discrete directions having index m. Later, the first term in the left hand side of Eq. (3) has been approximated using the backward differencing scheme in time. Hence, the discretized form of Eq. (3) can be written as [15, 22]:

$$\frac{\partial I_d^m(r,t)}{\partial s} + A I_d^m(r,t) = S_t^m(r,t) + B I_d^m(r,t-\Delta t) \tag{10}$$

where $B = 1/c\Delta t$ and $A = \beta(r) + B$ are the constants. Similarly, the boundary conditions for the one dimensional planar medium (Eq. (7)) in discrete directions can be written as:

$$I_d^m(r_w,t) = \frac{\varepsilon_w \sigma T_w^4}{\pi} + 2\pi\left(\frac{1-\varepsilon_w}{\pi}\right)\sum_{m=1}^{m=M_\theta/2}\left[I_d(r_w,\theta^m,t) + I_c(r_w,\theta^m,t)\right]\cos\theta^m \sin\theta^m \Delta\theta^m \tag{11}$$

where M_θ is the number of discrete points considered over the complete span of the polar angle θ ($0 \le \theta \le$ л), $M_\theta/2$ represents the angular space through which the incoming rays from the skin reaches the boundaries (the incident rays at the south boundary are coming from the north within the polar space ($0 \le \theta <$ л/2) and the incident rays at the north boundary are coming from the south within the polar space (л/2 < $\theta \le$ л)), and subscript w is a dummy variable for the north as well as the south boundaries. The resulting discretized equation of RTE, i.e., Eq. (10) is obtained by implementing FVM in all discrete directions m [22], and the intensity at the cell center of a control volume can be written as:

$$I_{d,p}^m(t) = \begin{cases} \dfrac{2D_z^m I_{d,N}^m(t) + S_{t,p}^m(t)dV\,\Delta\Omega^m + B I_{d,p}^m(t-\Delta t)dV\,\Delta\Omega^m}{2D_z^m + A\,dV\,d\Omega^m} & D_z^m > 0 \\ \dfrac{2\left|D_z^m\right| I_{d,S}^m(t) + S_{t,p}^m(t)dV\,\Delta\Omega^m + B I_{d,p}^m(t-\Delta t)dV\,\Delta\Omega^m}{2\left|D_z^m\right| + A\,dV\,d\Omega^m} & D_z^m < 0 \end{cases} \tag{12}$$

where D_z^m is the directional component of FVM (= 2π sin θ^m cos θ^m sin $\Delta\theta^m$) provided azimuth symmetry, $\Delta\Omega^m$ is the elemental solid angle in discrete direction (= 4π sin θ^m sin $\Delta\theta^m$/2), dV is the discrete volume (1×1×dz), superscripts P, N and S refer to cell center, north and south, respectively.

Owing to the azimuthal symmetry, the diffuse intensities at any point in the medium have to be traced over the polar space $0 \le \theta \le \pi$. From Eq. (12), the diffuse intensities are south bound for $0 \le \theta < \pi/2$ ($D_z^m > 0$), and northbound in the polar space for $\pi/2 < \theta \le \pi$ ($D_z^m < 0$). While marching from north to south ($D_z^m > 0$) the cell center intensity $I_{d,P}^m$ of the first control volume adjacent to the top boundary was determined at a particular direction, say m, using Eq. (12) based on the knowledge of north boundary intensity $I_{d,N}^m$ obtained from boundary condition (Eq. (11)). Next, based on the known value of cell center $I_{d,P}^m$ and north boundary $I_{d,N}^m$ intensities of the first control volume adjacent to the top boundary, the intensity $I_{d,S}^m$ at the common boundary of first and second control volume has been determined using the relation:

$$I_{d,P}^m(t) = \frac{I_{d,S}^m(t) + I_{d,N}^m(t)}{2} \tag{13}$$

Further, the known intensity $I_{d,S}^m$ of the first control volume will become the north intensity $I_{d,N}^m$ for the second control volume. Again, in a similar fashion, the intensity at the cell center $I_{d,P}^m$ and at the cell interface $I_{d,S}^m$ of second control volume were determined. This space marching process has been repeated for all the discrete directions ($0 \le \theta < \pi/2$), and for all the control volumes from the north boundary to the south boundary.

In a similar fashion, the cell center intensity $I_{d,P}^m$ for the first control volume adjacent to the bottom boundary has been determined using Eq. (12) while marching from south to north

$(D_z^m < 0)$ based on the knowledge of south boundary intensity $I_{d,S}^m$ using the boundary condition ((Eq. (11)). Next, based on the known value of cell center $I_{d,P}^m$ and north boundary $I_{d,S}^m$ intensities of the first control volume adjacent to the bottom boundary, the intensity $I_{d,N}^m$ at the common boundary of last and second last control volume has been determined using Eq. (13). Again, the known intensity $I_{d,N}^m$ of the last control volume will become the south intensity $I_{d,S}^m$ for the second last control volume, and the intensity at the cell center $I_{d,P}^m$ and at the cell interface $I_{d,N}^m$ of second last control volume was determined in similar fashion. Here also, the space marching process has been repeated for all the discrete directions ($\pi/2 < \theta \leq \pi$), and for all the control volumes from the south boundary to the north boundary.

At any time level, the computation of cell centre intensities also requires the knowledge of the total source terms and cell centre intensities of the previous time level, which are the implicit functions of the intensity. The values for the terms that are implicit function of intensities are taken as a guess during computation, which are refined by achieving a numerical convergence after repeated iterations. A detailed discussion on the ray tracing and time marching procedure can be obtained from [15, 22].

After the intensities are evaluated at all nodes and discrete angles, the distribution of reflected radiative heat flux at the irradiating surface is computed using Eq. (9). The boundaries of the skin have been assumed to be covered with a gel of similar refractive index of that of the tissues to avoid mismatch in the refractive index at air-tissue interface. The emission component of the radiation owing to the temperature of the skin and absorption of radiant energy including its boundary does not affect the radiative signatures. This is due to very short residence time of radiation in the skin {O (10^{-12} s)}. The absence of emission component as explained above, i.e., the nonexistence of reflection component, is owing to the fact that human skin acts like a black surface [15].

Each skin layer has been divided into equal cell size having grid size of 0.002 mm. The study considers 50 angular divisions of polar space. These parameters are identified after grid and ray independent study. The convergence at each time step (9.333×10^{-3} ps) has been assumed to have achieved when the change in the total source term S_t at all the points for two consecutive iterations did not exceed the tolerance limit (1.0×10^{-13}). In order to evaluate the accuracy of the FVM, the results obtained using FVM has been validated with that of the mDOM [15].

In the literature, the reflectance mode detection of subsurface anomalies within a mimicking tissue (or mouse models) has been extensively studied [7, 13, 14]. These studies were not specific to any human tissue and malignancies, and are of general nature or on mouse models. Also, significant number of studies related to numerical radiative transfer methods to this class of problems have been studied such as the Monte Carlo method [7], the discrete ordinate method [13-15], and the finite volume method [24].

RESULTS AND DISCUSSION

The variation of collimated (I_c^*) and directional diffuse intensities ($I_d^{m,*}$) along with the depth of healthy skin at different instants of laser exposure and idle time has been shown in Fig. 3.

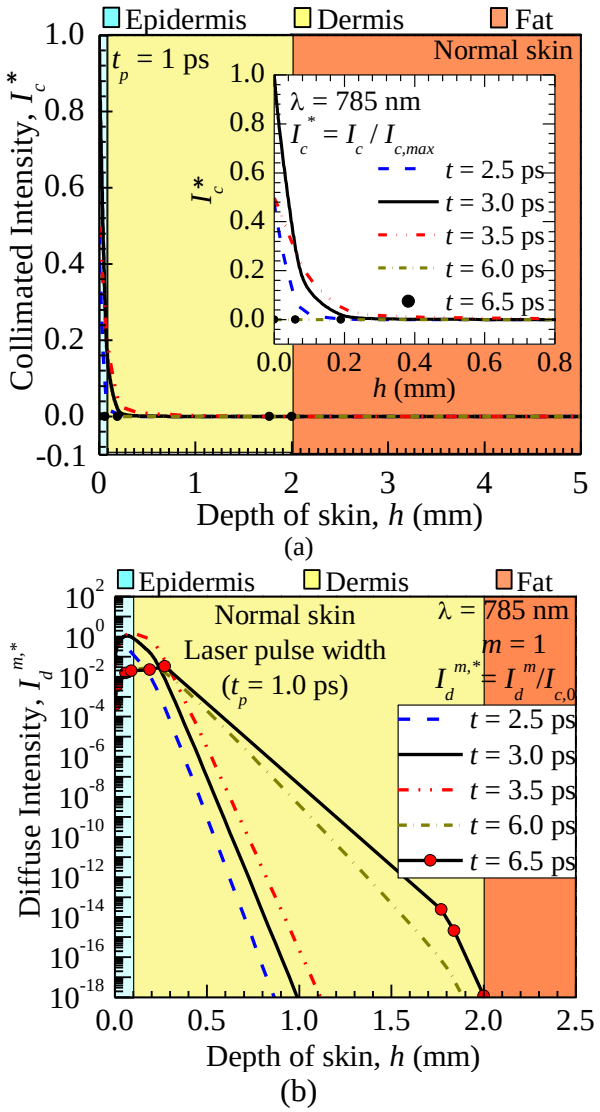

Figure 3 Variation of (a) the collimated intensity and (b) the directional diffuse intensity with the depth of healthy skin, h, subjected to a single laser pulse of 1ps pulse width. The intensity distributions with the depth have been presented for different instants of laser exposure, i.e., t = 2.5 ps, 3.0 ps, 3.5 ps, and 6.0 ps, and laser idle time of t = 6.5 ps

It can be observed from Fig. 3(a) that, the collimated intensity of laser light travels a distance of h = 0.2 mm (up to the papillary dermis) within the skin and completely disappears with further increase in the depth. The maximum magnitude of

collimated intensities along the depth has been observed at the peak of the Gaussian laser pulse, i.e., at t = 3.0 ps, when the skin is subjected to single laser pulse of 1 ps pulse width. The directional diffuse intensities ($I_d^{m,*}$) due to the attenuation of collimated remnant have been found to be penetrating to a greater distance, say, 2 mm (up to the lower dermal layer), within the skin as can be seen from Fig. 3(b). Hence, the diffuse intensity allows one to resolve greater probing depth. The contribution of south bound directional diffuse intensity along the incident direction, *i.e.*, m = 1, has been presented in Fig. 3(b) for different instants. The peak magnitude of the diffuse intensities ($I_d^{1,*}$) has been observed within few millimetres of the living epidermis, and the maximum value of the diffuse remnant along the depth has been observed at t = 3.5 ps of laser exposure time.

The reflected radiative signals from various stages of cutaneous melanoma (ES I, CL II, CL III and CL IV) as well as benign lesion (DPN) have been compared with that of the healthy skin in Fig. 4. Whereas, Fig. 5 depicts the variation in the relative contrast (Δq^*_{ref}) between the healthy skin ($q^*_{ref,norm}$) and different lesions ($q^*_{ref,lesion}$).

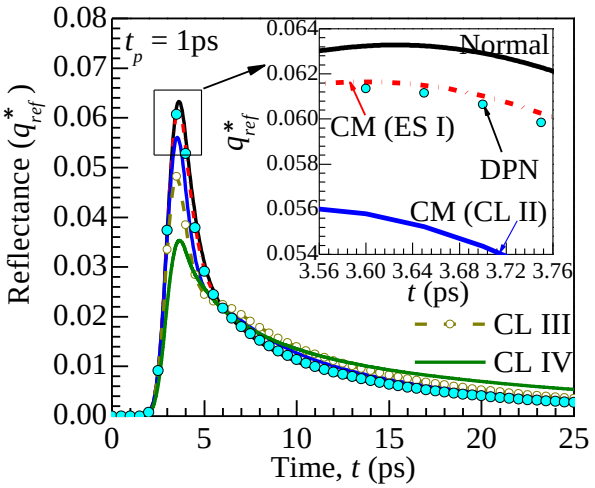

Figure 3 Temporal variations of reflectance (q^*_{ref}) from healthy skin, various stages of malignant lesions (ES I, CL II, CL III and CL IV) and benign lesion (DPN) due to SP laser light of 1 ps pulse width

It can be observed from Figs. 4 and 5 that, the increase in penetration depth with different stages of melanoma increases the difference between the peak magnitude of reflected signals emanating from healthy skin and melanoma.

The peak magnitude of characteristic signals from skin with DPN and different CM stages have also been found to be varying, except that for the early stage of CM (ES I), as can be seen from enlarged view of Fig. 4. It is evident from Fig. 4 that, the change in temporal variation of characteristic signals is an indicative of the CM spread to greater depths, and the variation in the relative contrast in Fig. 5 between different CM stages are clearly distinguishable. The observed change in the magnitude of characteristic signals is mainly due to difference in lesion absorption and scattering coefficient. Based on the above observations, it can be predicted that, the reflectance mode SP laser probing approach is capable to distinguish different growth phases of melanoma and benign lesion from the healthy skin, but the probing method fails to differentiate the benign from malignant. Overall the performance of reflectance mode SP laser modality has been found to be sensitive to the change in optical properties and penetration depth of lesion within the skin.

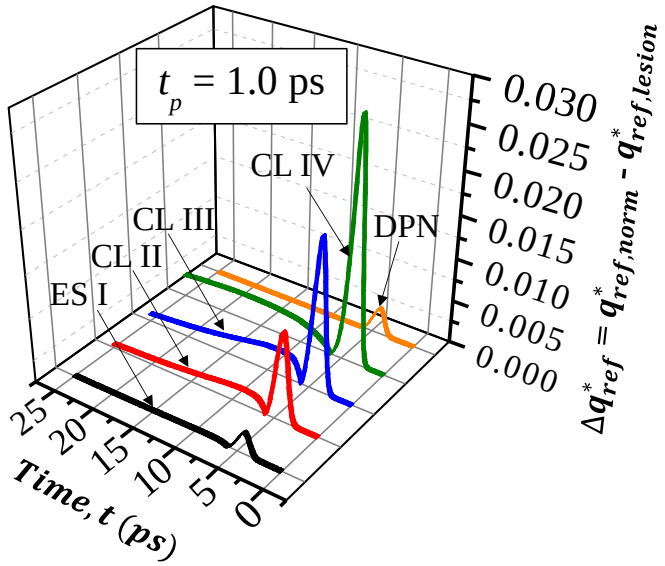

Figure 5 The temporal variation of the difference in the reflectance values, Δq^*_{ref} , between healthy skin ($q^*_{ref,norm}$) and various lesion ($q^*_{ref,lesion}$) within the skin

CONCLUSIONS

This paper presents a model based feasibility study to demonstrate the role of short-pulse laser for the detection and differentiation of skin melanoma stages and benign lesion. Here, the reflected signatures from normal human skin and skin with abnormal lesion were used (a) to differentiate different stages of cancer (melanoma) and (b) to distinguish melanoma from benign lesion. The study revealed that, the present short-pulse laser probing approach is capable to differentiate various growth phases of melanoma from the healthy skin except the early stage (ES I) that featured negligible contrast between the healthy skin and skin with ES I. In addition, the probing method also failed to distinguish the benign lesion (dysplastic nevi) from malignant lesion (melanoma) since their optical properties were nearly same. Overall, the performance of the present short-pulse laser modality has been found to be sensitive to the change in optical properties and penetration depth of lesion within the skin. Finally, the evaluation time for the present probing system is of the order of picosecond which is relatively fast compared to the other non-invasive skin cancer detection systems.

REFERENCES

[1] Psaty E.L., and Halpern A.C., Current and emerging technologies in melanoma diagnosis: the state of the art, *Clinics in Dermatology*, vol. 27, 2009, pp. 35-45.

[2] Rigel D.S., Russak J., and Friedman R., The evolution of melanoma diagnosis: 25 year beyond the ABCDs, *CA: A Cancer Journal for Clinicians*, vol. 60, 2010, pp. 301-316.

[3] Bafounta M.L., Beauchet A., Aegerter P., and Saiag P., Is Dermoscopy (Epiluminescence Mi-croscopy) useful for Diagnosis of Melanoma? Results of a Meta-analysis using Techniques Adapted to the Evaluation of Diagnostic Tests, *Archives of Dermatology*, vol. 137, 2001, pp. 1343-1350.

[4] Gerger A., Hofmann-Wellenhof R., Samonigg H., and Smolle J., In Vivo Confocal Laser Scan-ning Microscopy in the Diagnosis of Melanocytic Skin Tumours, *British Journal of Dermatology*, vol. 160, 2009, pp. 475-481.

[5] Li Y., Gonzalez S., Terwey T.H., Wolchok J., Li Y., Aranda I., Crow R.T., and Halpern A.C., Dual mode reflectance and fluorescence con-focal laser scanning microscopy for in vivo imaging melanoma progression in murine model, *Journal of Investigative Dermatology*, vol. 127, 2007, pp. 2184-2190.

[6] Gutkowicz-Krusin D., Elbaum M., Jacobs A., Keem S., Kopf A.W., Kamino H., Wang S., Rubin P., Rabinovitz H., and Oliviero M., Precision of automatic measure-ments of pigmented skin lesion parameters with a MelaFind multispectral digital dermo-scope, *Melanoma Research*, vol. 10, 2000, pp. 563-570.

[7] Guo Z., Wan S.K., August D.A., Ying J., Dunn S.M., and Semmlow J.L., Optical imaging of breast tumor through temporal log-slope difference mappings, Computers in Biology and Medicine, vol. 36, 2006, 209 -223.

[8] Blum A., Schmid-Wendtner M.H., Mauss-Kiefer V., Eberle J.Y., Kuchelmeister C., and Dill-Müller D., Ultrasound mapping of lymph node and subcutaneous metastases in patients with cutaneous melanoma: results of a prospective multicenter study, *Dermatology*, vol. 212, 2006, pp. 47-52.

[9] Mehrmohammadi M., Yoon S.J., Yeager D., and Emelianov S.Y., Photoacoustic imaging for cancer detection and staging, *Current Molecular Imaging*, vol. 2, 2013, pp. 89-105.

[10] Lui H., Zhao J., McLean D., and Zeng H., Real-time Raman spectroscopy for in vivo skin cancer diagnosis, *Cancer Research*, vol. 72, 2012, pp. 2491-2500.

[11] Sterenborg H.J.C.M., Motamedi M., Wagner Jr R.F., Duvic M., Thomsen S., and Jacques S.L., In vivo fluorescence spectroscopy and imaging of human skin tumours, *Lasers in Medicine and Science*, vol. 9,1994, pp. 191-201.

[12] Bhowmik A., Repaka R., and Mishra S.C., Thermographic evaluation of early melanoma within the vascularized skin using combined non-Newtonian blood flow and bioheat models, *Computers in Biology and Medicine*, vol. 53, 2014, pp. 206-219.

[13] Das C., Trivedi A., Mitra K., and Vo-dinh T., Experimental and numerical analysis of short-pulse laser interaction with tissue phantoms containing inhomogeneities, *Applied Optics*, vol. 42, 2003, pp. 16–19.

[14] Pal G., Basu S., Mitra K., and Vo-Dinh T., Time-resolved optical tomography using short-pulse laser for tumor detection, *Applied Optics*, vol. 45, 2006, pp. 6270-6282.

[15] Bhowmik A., Repaka R., Mishra S.C., and Mitra K., Analysis of radiative signals from normal and malignant human skins subjected to a short-pulse laser, International Journal of Heat and Mass Transfer, vol. 68, 2014, pp. 278-294.

[16] Greene F.L., Compton C.C., Fritz A.G., Shah J.P., and Winchester D.P., Melanoma of the Skin, In: AJCC Cancer Staging Atlas, Springer: New York, 2006, pp. 207-216.

[17] Bashkatov A.N., Genina E.A., and Tuchin V.V., Optical properties of skin, subcutaneous, and muscle tissues: a review, *Journal of Innovative Optical Health Science*, vol. 4, 2011, pp. 9−38.

[18] Simpson R.C., Kohl M., Essenpris E., and Cope M., Near-infrared optical properties on ex vi-vo human skin and subcutaneous tissues measured using Monte Carlo inversion technique, *Physics in Medicine and Biology*, vol. 43, 1998, pp. 2465−2478.

[19] Wang S., Zhao J., Lui H., He Q., and Zeng H., Monte Carlo simulation of near infrared autofluores-cence measurements of in vivo skin, *Journal of Photochemical and Photobiology B*, vol. 105, 2011, pp. 183−189.

[20] Garcia-Uribe A., Smith E.B., Zou J., Duvic M., Prieto V., and Wang L.V., In-vivo characterization of optical proper-ties of pigmented skin lesions including melanoma using oblique incidence diffuse reflec-tance spectrometry, Journal of Biomedical Optics, vol. 16, 2011, pp. 0205011−0205013.

[21] Modest M.F., Radiative Heat Transfer, second ed., 2003, New York.

[22] Mishra S.C., Chungh P., Kumar P., and Mitra K., Development and comparison of the DTM, the DOM and the FVM formulations for the short-pulse laser transport through a participating medium, International Journal of Heat and Mass Transfer, vol. 49, 2006, pp. 1820−1832.

[23] Muthukumaran R., and Mishra S.C., Analysis of the transport of a train of short-pulse radiation of Gaussian temporal profile through a 2-D participating medium, *Heat Transfer Engineering*, vol. 30, 2009, vol. 1197-1207.

[24] Chai J.C., Hsu P.-F., and Lam Y.C., Three-dimensional transient radiative transfer modeling using the finite-volume method, *Journal of Quantitative Spectroscopy and Radiative Transfer*, vol. 86, 2004, pp. 299–313.